The Jahn–Teller effect in Cr^{5+}-doped $PbTiO_3$: a multi-frequency electron paramagnetic resonance study

2010 J. Phys.: Condens. Matter 22 065902

(http://iopscience.iop.org/0953-8984/22/6/065902)

J. Phys.: Condens. Matter **22** (2010) 065902 (8pp) doi:10.1088/0953-8984/22/6/065902

The Jahn–Teller effect in Cr^{5+}-doped $PbTiO_3$: a multi-frequency electron paramagnetic resonance study

R Böttcher[1,3], A Pöppl[1], J Hoentsch[1] and R M Rakhmatullin[2]

[1] Fakultät für Physik und Geowissenschaften, Universität Leipzig, Linnéstraße 5, D-04103 Leipzig, Germany
[2] MRS Laboratory, Kazan State University, Kremlevskaya 18, 420008 Kazan, Russia

Received 1 September 2009, in final form 22 December 2009
Published 27 January 2010
Online at stacks.iop.org/JPhysCM/22/065902

Abstract
Electron paramagnetic resonance (EPR) spectra of Cr^{5+} defects incorporated on Ti^{4+} sites in powdered ceramics of $PbTiO_3$ were investigated in the temperature range 50–400 K at 9 GHz (X), 34 GHz (Q) and 94 GHz (W band). The $T_2 \otimes e$ Jahn–Teller effect stabilizes the vibronic ground state of the $3d^1$ electron of the Cr^{5+} ion and leads to a tetragonally distorted defect-O_6 octahedron with the point symmetry D_{4h}. The spontaneous electrical polarization present in the ferroelectric phase of $PbTiO_3$ appears as a further perturbation producing an additional g-tensor contribution by the quadratic field effect. Its symmetry is dependent on the orientation of the electrical polarization with respect to the Jahn–Teller distortion axis, the tetragonal axis of the defect-O_6 octahedron. If the polarization of a domain is anti- or parallel to this axis, the local tetragonal symmetry of the Cr^{5+} ion persists whereas it is reduced by a perpendicular orientation. Anisotropic EPR spectra of tetragonally and orthorhombic distorted $Cr^{5+}O_6^{12-}$ are detected at low temperatures. Increasing the temperature, the peaks of the two spectra are broadened and a motionally averaged isotropic spectrum appears at 200 K.

1. Introduction

For the ferroelectric perovskites ($BaTiO_3$, $PbTiO_3$, $PbZrO_3$ and their mixed systems), an advantage is that their physical and chemical properties may be selectively tailored by doping with transition-metal and rare-earth ions on a percentage level. Therefore, the understanding of physical and chemical properties of such doping centres in these materials is of interest for fundamental reasons and for the technological applications ranging from ferroelectric non-volatile memory devices to piezoelectric actuators [1–5]. Information concerning the effects of processing conditions such as temperature, dopant type and concentration on defect charge state and site location are of particular importance to optimize the perovskitic materials for further applications. Here we use the multi-frequency electron paramagnetic resonance (EPR) spectroscopy, a well-established technique for probing the site location and its symmetry as well as the electronic structure of paramagnetic ions and defects in single- and polycrystalline solids, to study the incorporation of Cr^{5+} ions into the $PbTiO_3$ lattice.

In the barium titanate lattice two possibilities of the incorporation of paramagnetic Cr^{5+} ions (electron configuration $3d^1$ with the free-ion ground state ^2D) exist: octahedrally and quasi-tetrahedrally coordinated Cr^{5+} [6–10]. In the case of the octahedrally coordinated Cr_I^{5+} defect the tetragonal Jahn–Teller distortion of the $Cr^{5+}O_6^{12-}$ complex is weakly disturbed by a *quadratic* field effect of the electrical polarization in the ⟨111⟩ directions at low temperatures (rhombohedral phase). The tetragonal D_{4h} symmetry of the complex is reduced and EPR spectra with rhombic symmetry are detected in the rhombohedral phase. The abnormal position of the principal axes of the g tensor can be accounted for by a polarization model [9]. The quasi-tetrahedral coordination of the Cr_{II}^{5+} ion arises through a displacement of chromium along a [110] direction. Hence, the ion becomes quasi-tetrahedrally coordinated by four O^{2+} ions. A *linear* coupling of the electric spontaneous polarization P^S and the electric dipole moments, associated with an off-centred ion within the octahedron of surrounding O^{2-} ions, induces the alignment of the dipoles

[3] Author to whom any correspondence should be addressed.

and polarization-dependent g tensors. This coupling causes a doublet splitting of the peaks in the EPR powder spectrum of the quasi-tetrahedrally coordinated Cr^{5+} defect [10].

In cubic $SrTiO_3$, two different EPR spectra of Cr^{5+} ions have also been observed, which are explained by different impurity sites with either tetragonal or orthorhombic local symmetry [11, 12]. In the presence of uniaxial stress and external electrical fields, EPR studies of Cr^{5+} with locally tetragonal surroundings confirmed that the octahedral–tetragonal reduction of the site symmetry is caused by the $T_2 \otimes e$ static Jahn–Teller effect [12, 13]. In the case of Cr^{5+} with a rhombic site symmetry, Müller showed that the defect ion corresponds to an off-centre case, in which Cr^{5+} is transformed from an octahedral into a tetrahedral site through a displacement along one of the ⟨110⟩ crystallographic directions [14]. From EPR measurements in the presence of external electric fields the dipole moment associated with the off-centred Cr^{5+} ion and its displacement has been determined [15].

The first EPR and ENDOR measurements on chromium-modified $PbTiO_3$ ceramics, published in 1986, showed that Cr^{5+} is incorporated in crystalline regions of the $PbTiO_3$ grain ceramics at Ti^{4+} sites. The symmetry of the impurity is lower than that of the host Ti^{4+} sites. An explanation of the symmetry reduction was not given [16]. Recent methodological advances concerning the use of high frequencies [17] and improved computer programs for the simulation of polycrystalline powder EPR spectra [18–20] have allowed us to reanalyse the complicated powder spectrum of Cr^{5+}-doped $PbTiO_3$ and to determine its spin-Hamiltonian parameters. In this work we show that the Cr^{5+} spectrum can be dissected into two distinct subspectra with tetragonal and rhombic symmetry. The different local symmetries of Cr^{5+} ions are explained by the Jahn–Teller distortion and the additive influence of the spontaneous electric polarization of the ferroelectric domains on the position of the Cr^{5+} ions and on their local O^{2-} surroundings.

2. Crystal structure and Cr^{5+} spin-Hamiltonian

$PbTiO_3$ belongs to the important group of ferroelectric materials based on the cubic ABO_3 perovskite structure. At the temperature of 765 K $PbTiO_3$ undergoes a single-phase transition from the paraelectric cubic phase to a tetragonally distorted ferroelectric phase and remains in this tetragonal phase with the space group $P4mm$ down to low temperatures. In this state, six energetically equivalent orientations of the spontaneous polarization exist along the ⟨100⟩ axes (index referring to the cubic paraelectric phase). The structure of pure $PbTiO_3$ has been investigated in the ferroelectric phase at 90, 158 and 298 K and in the paraelectric cubic phase (symmetry group $Pm3m$) at 823 by Glazer *et al* [21]. With the Pb atom at the origin, the positions of all atoms in the unit cell are described by three temperature-dependent position parameters δz_{Ti}, $\delta z_{O(1)}$, $\delta z_{O(2)}$. The coordinates of the atoms in the unit cell are: Pb at (0, 0, 0), Ti at (0.5, 0.5, $0.5 + \delta z_{Ti}$), O(1) at (0.5, 0.5, $\delta z_{O(1)}$), and O(2) at (0.5, 0, $0.5+\delta z_{O(2)}$) and (0, 0.5, $0.5+\delta_{O(2)}$) (table 1). In the ferroelectric phase, the oxygen octahedron is elongated along the c axis (direction of the polarization) and also shifted by 0.54 Å with respect to the Pb^{2+} position, whereas the titanium is displaced from the centre of the cell along c by 0.17 Å, respectively. As a result, the titanium ion occupies an off-centre position within the shifted oxygen octahedron and has four nearest Pb neighbours and four next-nearest Pb neighbours. High-resolution synchrotron powder diffraction experiments were carried out at 12 K by Schönau *et al* [22] and confirmed the tetragonal symmetry group $P4mm$ with lattice parameter ratio (c/a ratio) of 1.0721, also in the low-temperature range. Size considerations of the ions in ABO_3 perovskite structures lead to the expectation that the 3d transition-metal ions are mainly incorporated at Ti sites (B site).

Table 1. Positional parameters δz_{Ti}, $\delta z_{O(1)}$, $\delta z_{O(2)}$ and lattice constants a, c in dependence on the temperature; all values in Å.

	90 K	158 K	298 K	823 K
δz_{Ti}	0.167	0.171	0.162	0
$\delta z_{O(1)}$	0.492	0.479	0.473	0
$\delta z_{O(2)}$	0.505	0.504	0.486	0
a	3.895	3.899	3.905	3.970
c	4.171	4.167	4.156	3.970

The Cr^{5+} spectra of isotopes without nuclear magnetic moments ($^{50,52,54}Cr$) are described by an $S = 1/2$ spin-Hamiltonian consisting only of the anisotropic Zeeman term

$$\hat{H} = \beta \vec{B} \underline{\underline{g}} \hat{\vec{S}}, \tag{1}$$

with $\underline{\underline{g}}$ the electronic g tensor (symmetric) and β the Bohr magneton, respectively. The isotope ^{53}Cr (natural abundance 9.5%) has the nuclear spin $^{53Cr}I = 3/2$. Due to its hyperfine interaction with the d^1 electron additional satellite peaks of low intensity occur in the powder pattern, which flank the peaks of the isotopes without nuclear moments. Furthermore, in the case of $PbTiO_3$, the spin-Hamiltonian must be augmented by the superhyperfine structure (SHFS) interaction of the $3d^1$ electron with the nuclear spin $I = 1/2$ of the ^{207}Pb neighbours. If the SHFS interaction is assumed to be isotropic, as indicated by the experimental EPR results, the four nearest ^{207}Pb nuclei (in relation to the Cr^{5+} lattice site) are all magnetically equivalent. The terms in the Hamiltonian that contribute to the SHFS are given by

$$\hat{H}_{SHFS} = \sum_i^n (A \hat{\vec{S}} \hat{\vec{I}}_i - g_{^{207}Pb} \beta_N \vec{B} \hat{\vec{I}}_i), \tag{2}$$

with A the isotropic SHFS coupling constant, $g_{^{207}Pb}$ the nuclear g factor for ^{207}Pb nuclei and β_N the nuclear magneton, respectively. However, not all sites are equivalent in their nuclear surroundings, because the lead isotope ^{207}Pb has a natural abundance of only 22.1%, the other isotopes having zero nuclear spin. The probability of occupation of a lead site by a ^{207}Pb is 0.221. Provided that the Cr^{5+} ion is incorporated on the Ti lattice site, the resulting spectrum is an overlap of five subspectra with $n = 0, 1, \ldots, 4$ in (2). Their relative

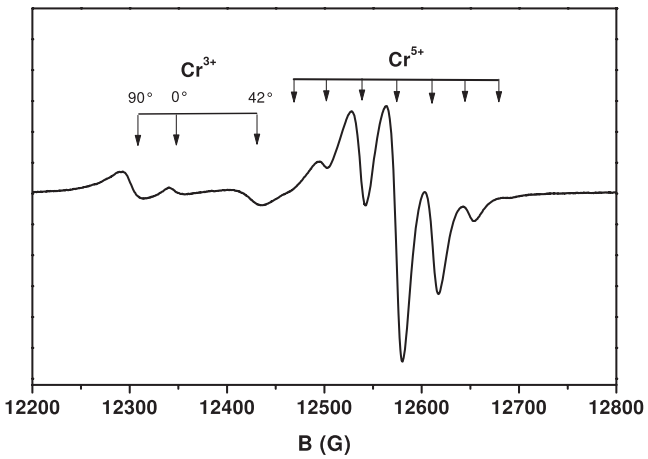

Figure 1. EPR spectrum of the Cr-doped $PbTiO_3$ measured at 300 K and 34 GHz (Q band). In the low-field part of the spectrum the peaks of the central transition $M_S = 1/2 \leftrightarrow M_S = -1/2$ of the C1–Cr^{3+} spectrum are visible. The isotropic Cr^{5+} line is split by superhyperfine structure interaction with the nuclear magnetic moments of ^{207}Pb nuclei.

intensities are given by

$$w(n) = \frac{4!}{n!(4-n!)} p_0^n p_E^{4-n}, \tag{3}$$

with $p_0 = 0.221$ and $p_E = 0.778$. Assuming isotropic g and A values in (1) and (2) a seven-line pattern with relative intensities

0.009:0.098:0.484:1:0.484:0.098:0.009

is expected in the resulting spectrum in which the distance of two neighbouring lines is given by $A/2$.

For the determination of the spin-Hamiltonian parameters and the evaluation of the ceramic powder EPR spectra the MATLAB[4] toolbox for electron paramagnetic resonance 'easy spin 2.0.3' was used [18–20]. By simulating the polycrystalline powder spectra by variation of the parameters of the spin Hamiltonians (1) and (2) for the 1/2-spin system Cr^{5+} with ^{207}Pb SHFS interaction, a satisfactory accuracy in the determination of the spectral parameters was achieved. In ceramics, where the local crystal field undergoes random fluctuations, a single set of spin-Hamiltonian parameters is inadequate for the description of paramagnetic defect centres and rather a distribution of the spin-Hamiltonian parameters is needed. For the Cr^{5+} ion we used only the distribution of the principal values of the g tensor in the simulation of the powder spectra. Assuming random fluctuations in the local lattice parameters in the vicinity of the paramagnetic impurity these distributions can be approximated by a Gaussian lineshape with the full widths at half-height (FWHH) Δg_1, Δg_2 and Δg_3.

3. Experimental details

Ceramic powders with the nominal composition $PbTiO_3 + 0.05PbO + 0.01Cr_2O_3$ were prepared by the conventional mixed-oxide powder technique. After mixing (agate balls, water) and calcining (1173 K, 2 h) of PbO, TiO_2 and Cr_2O_3 the $PbTiO_3$ powder was fine-milled (agate balls, 2-propanol) and densified to discs with a diameter of 6 mm and a height of nearly 3 mm. The samples were sintered in air at a temperature of 1473 K for 2 h (heating rate 10 K min^{-1}). The overall phase composition was checked by XRD at room temperature. All samples were in the single-phase state.

EPR measurements of the pulverized ceramics samples were carried out at the X (9.4 GHz), Q (34 GHz) and W (94 GHz) frequency band with Bruker spectrometers (ELEXSYS E580, EMX and ELEXSYS E680). Temperatures between 5 and 400 K were achieved with an Oxford flowing He gas cryostat in connection with an Oxford ITC controller (temperature stability about 0.2 K) and a variable temperature accessory E 257 (Varian, temperature stability about 1 K). More details of the measuring procedure are given in [9].

[4] MATLAB is a registered trademark of MathWorks, Inc., Natick, MA, USA.

Table 2. Principal values and the FWHH of the distributions of the g tensors for the tetragonal t-Cr^{5+} and rhombic o-Cr^{5+} centre in the tetragonal phase of $PbTiO_3$. For comparison the values of the Cr_I^{5+} centre in the orthorhombic phase of $BaTiO_3$ are also given. The experimental error of the g values is ± 0.0003, and for FWHH it is ± 0.0002.

	T (K)	g_1	g_2	g_3	Δg_1	Δg_2	Δg_3
iso-Cr [a]	300		1.9358		—	—	—
t-Cr^{5+} [a]	50	1.9360	1.9360	1.9404	0.0005	0.0003	0.0003
o-Cr^{5+} [a]	50	1.9300	1.9360	1.9483	0.0028	0.0018	0.0018
Cr_I^{5+} [b]	50	1.9347	1.9533	1.9596	0.0030	0.0015	0.0007

[a] This work. [b] Data for $BaTiO_3$ taken from [9].

4. Results

Figure 1 shows the EPR spectrum of a Cr-doped, powdered ceramic $PbTiO_3$ sample in the tetragonal phase ($T = 300$ K) measured at 34 GHz (Q band). The three weak peaks in the low-field part of this spectrum are assigned to the central transition $M_S = 1/2 \leftrightarrow M_S = -1/2$ of the axial Cr^{3+} (electron spin $S = 3/2$) spectrum of the C1 centre [23–25]. Due to the axial fine structure (fs) parameter ($D = 0.0840$ cm^{-1}) of this centre the three peaks belonging to the canonical orientations $\theta = 0°$, 42° and 90° are observable in the X- and Q-band powder spectra, and θ is the angle between the static magnetic field and the symmetry axis of the C1 centre, the c axis of the $PbTiO_3$ lattice.

The seven lines with relative intensity ratio 0.01:0.09:0.48:1:0.48:0.09:0.01 belong to a nearly isotropic Cr^{5+} ($S = 1/2$) spectrum with $g_{iso} = 1.9358$. The frequency-independent splitting is caused by SHFS interaction of the unpaired $3d^1$ electron of the Cr^{5+} ions with the nuclear spin of the ^{207}Pb neighbours. Under the assumption that the Cr^{5+} ion has only four nearest Pb neighbours and the SHFS interaction is isotropic ($A_{iso} = (68 \pm 1)10^{-4}$ cm^{-1}), the simulated X-, Q- and W-band spectra are in accordance with the experimental ones.

With decreasing temperature, a strong reduction of the widths of SHFS lines of the Cr^{5+} spectrum is observed. At 70 K each SHFS line shows a splitting into several peaks.

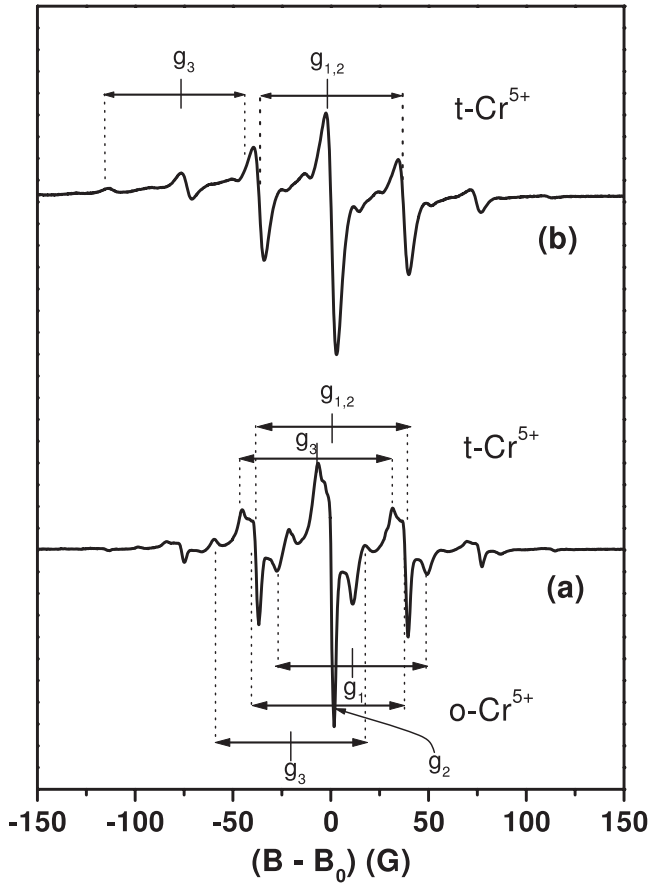

Figure 2. X- (a) and W-band (b) spectrum of Cr^{5+} ions in ceramic-powdered $PbTiO_3$ measured at 50 K. The g-positions of the tetragonal and rhombic spectra were marked, $B_0 = \frac{h\nu}{\beta g_2}$, ν microwave frequency, g_2 is given in table 2.

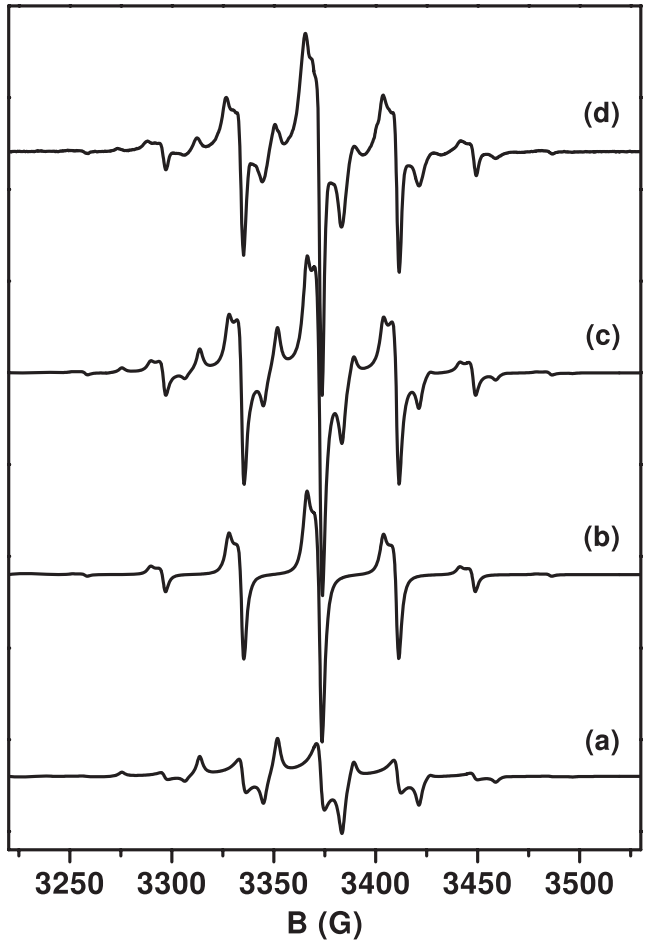

Figure 3. Simulation of the X-band spectrum of the Cr^{5+} ions. For the simulation the spin-Hamiltonian parameters given in table 2 were used. Simulated rhombic powder spectrum (a), simulated tetragonal powder spectrum (b), sum of the tetragonal and rhombic spectrum (c) as well as the experimental spectrum (d). The ^{53}Cr hyperfine structure was neglected in the simulation.

The number of the conspicuous peaks in the powder pattern is dependent on the microwave frequency. The X- and W-band spectra of the ceramic powder are depicted in figure 2; the number of the peaks in the W-band spectrum is reduced. Extensive simulations (figures 3 and 4) have been necessary to understand the complicated structures of the powder spectra and to explain the disappearance of the peaks in the W-band spectrum. The results of the simulation process are: the X-band spectrum (figure 2(a)) is an overlap of a tetragonal and orthorhombic powder pattern, whereas only the tetragonal powder pattern is visible in the W-band spectrum (figures 2(b) and 4). Each of them can be decomposed into five subspectra corresponding to the number n ($n = 0, 1, \ldots, 4$) of ^{207}Pb nuclei in the first Pb shell. In figure 2(a) the peaks of the powder spectra of Cr^{5+} ions in tetragonal and orthorhombic local symmetry with essentially $n = 1$ (only one Pb nucleus has a nuclear spin in the first shell) are marked. A deviation of the magnetic equivalence of the nearest Pb nuclei could not be determined ($A_{iso} = (67.5 \pm 0.8)10^{-4}$ cm^{-1}), the anisotropic part of the SHFS parameter is less than 10^{-4} cm^{-1}. In the W-band spectrum each peak of the perpendicular part of the tetragonal powder pattern is flanked by two satellites (in figure 4(b) marked by asterisks), which arise from the ^{53}Cr hyperfine structure interaction with the coupling constant $^{53Cr}A = (7.5 \pm 0.6)10^{-4}$ cm^{-1}. Because of the width of the main peaks (about 6 G) only the hyperfine transitions with the nuclear spin quantum numbers $m = \pm 3/2$ are resolved. Other reasons for the appearance of these weak peaks, based on higher-order hyperfine effects (spin–flip transitions), can be excluded due to the small magnetic moment of the ^{207}Pb nuclei and the high field in the W-band experiment. The widths of all peaks are broadened by a g-strain effect. For the tetragonal and orthorhombic spectra the g-strain parameters are different. By simulation of the X- (figure 3) and W-band (figure 4) spectra the spin-Hamiltonian parameters and the g-strain parameters were determined and are given in table 2. The substantial g-strain effects of the orthorhombic Cr^{5+} centre lead to an increasing broadening of its spectrum with rising frequency and in that way prevent its detection at 94 GHz (figure 4).

5. Discussion

Chromium ions are incorporated into the perovskite lattice on the B sites as Cr^{2+} (electron configuration $3d^4$ with the free-ion ground state ^5D), Cr^{3+} ($3d^3$, ^4F), Cr^{4+} ($3d^2$, ^3F) and/or

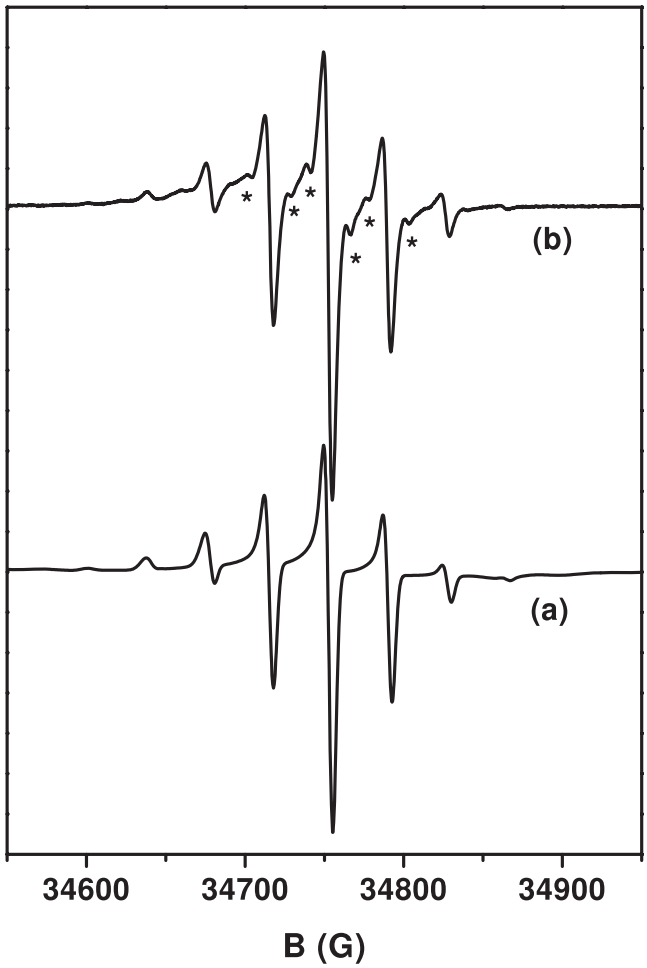

Figure 4. W-band spectrum of the Cr^{5+} ions: the simulated tetragonal spectrum (a) in comparison with the experimental spectrum (b). Due to the g strain in the rhombic spectrum its peaks are broadened and therefore they are not detectable in the experimental spectrum. The ^{53}Cr hyperfine structure peaks, which are resolved in the perpendicular part of the W-band powder pattern and marked by asterisks, were neglected in the simulation process.

Cr^{5+} ($3d^1$, ^2D). In the high-temperature (paraelectric) phase of these crystals the ions are surrounded by six oxygen ions forming a regular octahedron. Owing to the local electrical crystal field with cubic symmetry the orbital degeneracy of the free-ion states is partially lifted [26]:

$$^5D(Cr^{2+}) \longrightarrow {}^5E_g(Cr^{2+}) + {}^5T_{2g}(Cr^{2+})$$

$$^4F(Cr^{3+}) \longrightarrow {}^4A_{2g}(Cr^{3+}) + {}^4T_{2g}(Cr^{3+}) + {}^4T_{1g}(Cr^{3+})$$

$$^3F(Cr^{4+}) \longrightarrow {}^3T_{1g}(Cr^{4+}) + {}^3T_{2g}(Cr^{4+}) + {}^3A_{2g}(Cr^{4+})$$

$$^2D(Cr^{5+}) \longrightarrow {}^2T_{2g}(Cr^{5+}) + {}^2E_g(Cr^{5+}).$$

Only in the case of Cr^{3+} ions is the ground state a non-degenerate orbital state ($^4A_{2g}$) whose spin degeneracy is removed by the spin–orbit interaction in combination with the crystalline electrical field of lower than cubic symmetry. Cr^{3+} ions ($S = 3/2$) are detectable by EPR in the cubic as well as the tetragonal phase of $PbTiO_3$. Three Cr^{3+} defect centres (C1, C2 and C3) with different axial fine structure splitting were identified in ceramic samples. In the material studied here only the C1 spectrum was observed. In the ferroelectric phase the axial fine structure parameter $D \propto (P^S)^2$ and the symmetry axis of the fs tensor is the polar axis [25, 27]. In contrast to Cr^{3+} the di-, tetra- and pentavalent chromium ions have doubly and triply orbital-degenerate ground states with the symmetries E, T_1 and T_2, respectively. According to the Jahn–Teller (JT) theorem such degenerate states are unstable with respect to small displacements of the neighbouring ions which lower the symmetry of the crystal field experienced by the paramagnetic centre [28].

The magnetic properties of JT ions with nd^1 electron configurations were investigated in detail in $SrTiO_3$:Cr^{5+} [11–15], $SrTiO_3$:V^{4+} [29, 30], $SrTiO_3$:Mo^{5+} [31], $BaTiO_3$:Ti^{3+} [9, 32–34] and $BaTiO_3$:Mo^{5+} [34, 35]. The prevailing tetragonal symmetry and the magnetic parameters of nd^1 ions could consistently be explained assuming a JT coupling between the $^2T_{2g}$ electronic ground state with a localized phonon mode of e symmetry in the strong coupling regime ($T_2 \otimes e$ JTE) [36]. Owing to the interaction of the phonon modes Q_θ and Q_ε (two-dimensional representation e) of the octahedral complex with the triply degenerate ground state $^2T_{2g}$ (wavefunctions xy, yz, zx), its local symmetry is reduced from cubic to tetragonal by distortion along one of the three cubic axes ([100], [010], [001]). The ground state is now an orbital singlet and its energy is lowered by the JT energy [36]

$$E_{JT} = \frac{V^2}{2\mu\omega^2} \tag{4}$$

with the effective mass μ of the phonon mode with the frequency ω. V characterizes the strength of the JT coupling. The maxima of the probability density of the unpaired 3d electron are lying in the plane perpendicular to the deformation direction. For an arbitrary orientation of the magnetic field with respect to the crystallographic axes, three EPR lines are observed in the spectrum, which are assigned to nd^1 defects with different orientations of the JT distortion. The principal values of the g tensor are [36]

$$g_\parallel = 2 - \frac{8k\lambda}{\Delta_4} \qquad \text{and} \qquad g_\perp = 2 - \frac{2k\lambda}{\Delta_1}. \tag{5}$$

The spin–orbit coupling is proportional to the constant λ being positive for one d electron. k is the orbital reduction factor and Δ_4 represents the splitting between the d_{xy} (ground state) and the $d_{x^2-y^2}$ level and can be approximated by the crystal field splitting in the cubic, undistorted precursor state. Δ_1 is the splitting of the T_2 state due to the JTE. The presence of the JTE was unambiguously proved by the behaviour of the crystals under uniaxial stress [34]. In such an experiment, the number of the occupied d orbitals extending perpendicular to the stress axis increases at the cost of the others.

To explain the complexity of the spectrum of the Cr^{5+} defects in $PbTiO_3$, one must consider the crystal structure of the ferroelectric phase together with the existence of domains, additional to the assumption of the JT distortion. The shape

and the symmetry of unit cells and domains of ferroelectrics in thermal equilibrium are mainly determined by spontaneous strain, which are the components S_{ik} of the symmetric strain tensor [37]:

$$S_{ik} = \sum_{m,n} Q_{mnik} P^{\mathrm{s}}_m P^{\mathrm{s}}_n. \tag{6}$$

Their occurrence is the direct consequence of the existence of the spontaneous electric polarization with the components P^{s}_m. The quantities Q_{mnik} are the elements of the electrostriction tensor of cubic lead titanate. The deformations are quadratic in the spontaneous polarization due to the centrosymmetric high-temperature phase (paraelectric) of lead titanate. In the polar phase the vector $\vec{P}^{\mathrm{s}}$ is oriented along one of the fourfold (tetragonal) axes of the pseudocubic unit cell. In order that the macroscopic symmetry of a multi-domain crystal in the low-temperature phase agrees with the point group of the high-temperature one, the domains of the polar phase must be arranged according to the six equivalent directions of the spontaneous polarization.

In the paraelectric phase with cubic symmetry, the $Cr^{5+}O_6^{12-}$ complexes are tetragonally distorted along the direction of one C_4 axis by the JT effect. The JT coupling is an internal interaction in a solid. Therefore, all equivalent directions occur with equal probability. In the ferroelectric phase, the spontaneous polarization is considered as an ancillary structural perturbation of the JT-distorted $Cr^{5+}O_6^{12-}$ complexes and generates an off-centre shift of the Cr^{5+} ions along the axes of the electrical polarization towards to the nearest plane of the Pb^{2+} ions. It induces charge displacements in the paramagnetic complex and changes the electronic wavefunctions of the Cr^{5+} ion. Therefore the polarization-induced interaction has to take into account by an additional Zeeman term to the spin Hamiltonian of the Cr^{5+} centre (1). We have to note that in the case of Cr^{3+} (C1 centre) such effects will mainly change the fs interaction which dominates the spectrum of this $S = 3/2$ ion. Because the symmetry group of the JT-defect centre is D_{4h} (fourfold symmetry axis $\parallel z$) only a quadratic polarization effect is expected. The polarization-dependent Zeeman energy may be described by

$$\hat{H}^{\mathrm{s}} = \beta \sum_{i,j,k,l} T_{ijkl} P^{\mathrm{s}}_i P^{\mathrm{s}}_j B_k \hat{S}_l = \beta \sum_{k,l} g^{\mathrm{s}}_{kl} B_k \hat{S}_l, \tag{7}$$

where

$$g^{\mathrm{s}}_{kl} = \sum_{i,j} T_{ijkl} P^{\mathrm{s}}_i P^{\mathrm{s}}_j \tag{8}$$

are the polarization-dependent g^{s} tensor components [38]. For the point symmetry D_{4h} of the defect centre the relevant fourth-rank tensor takes the form [39]

$$T_{ijkl} = \begin{pmatrix} T_{11} & T_{12} & T_{13} & & & \\ T_{12} & T_{11} & T_{13} & & & \\ T_{13} & T_{13} & T_{33} & & & \\ & & & T_{44} & & \\ & & & & T_{44} & \\ & & & & & T_{66} \end{pmatrix}. \tag{9}$$

The indices refer to the Voigt notation ($1 = xx$, $2 = yy, \ldots, 6 = xy = yx$ with the pseudocubic axes x, y and z). The z axis is the tetragonal symmetry axis of the defect centre, the axis of the JT distortion. Due to the quadratic field effect, the $Cr^{5+}O_6^{12-}$ centres in domains whose polarization directions are related by inversion symmetry have the same g^{s} tensor. Depending on the orientation of the JT distortion with respect to the direction of the electrical polarization two kinds of g^{s} tensors with different symmetry (tetragonal $\mathrm{s} = \mathrm{t}$ and orthorhombic $\mathrm{s} = \mathrm{o}$) are generated. If the vector of the spontaneous polarization is anti- or parallel to the JT distortion axis, the tetragonal symmetry of the g tensor of the JT-distorted $Cr^{5+}O_6^{12-}$ centres is conserved, but its principal values are shifted by the elements

$$g^{\mathrm{t}}_{xx} = g^{\mathrm{t}}_{yy} = (P^{\mathrm{s}})^2 (T_{13}) \qquad g^{\mathrm{t}}_{zz} = (P^{\mathrm{s}})^2 (T_{33}). \tag{10}$$

If the spontaneous polarization is perpendicularly directed to the JT distortion axis the tetragonal symmetry of the g tensor is reduced to an orthorhombic one. The shifts of the principal values are given by

$$g^{\mathrm{o}}_{xx} = (P^{\mathrm{s}})^2 (T_{11}) \qquad g^{\mathrm{o}}_{yy} = (P^{\mathrm{s}})^2 (T_{12}) \qquad g^{\mathrm{o}}_{zz} = (P^{\mathrm{s}})^2 (T_{13}). \tag{11}$$

Because the principal values $g_\parallel$ and $g_\perp$ of the JT-distorted $Cr^{5+}O_6^{12-}$ complex are unknown in the cubic phase, the estimation of the elements T_{ik} in (10, 11) from the experimental g values is unfeasible.

The effect of the spontaneous electrical polarization on the intensities of the tetragonal and orthorhombic powder patterns can only be discussed qualitatively. Due to the strong overlap of the peaks in the experimental powder spectrum the exact determination of the intensities of the two spectral types is not feasible. The triply degenerate vibronic ground state of the $T_2 \otimes \mathrm{e}$ JT system is very sensitive to strain and its degeneracy is lifted by the electrical polarization due to electrostrictive couplings. The ground state Hamiltonian of the strain perturbation is given by

$$\hat{H}_{\mathrm{St}} = V_{\mathrm{S}} (e_\theta \varepsilon_\theta + e_\varepsilon \varepsilon_\varepsilon), \tag{12}$$

where V_{S} is the strain coupling coefficient, and ε_θ and ε_ε are two standard orbital operators (3×3 matrices) belonging to the e representation [36]. The variables e_θ and e_ε are the strain components defined by $e_\theta = e_{zz} - \frac{1}{2}(e_{xx} + e_{yy})$ and $e_\varepsilon = \frac{1}{2}\sqrt{3}(e_{xx} - e_{yy})$. The polarization-induced strain components are given as $e_{ij} = \sum_{k,l} q_{ijkl} P^{\mathrm{s}}_k P^{\mathrm{s}}_l$. The unknown quantities q_{ijkl} are the elements of the electrostriction tensor (fourth-rank tensor) of the $Cr^{5+}O_6^{12-}$ complex embedded in the $PbTiO_3$ lattice. This tensor has the same symmetry as the tensor T_{ijkl} in equation (9). One obtains $e_{xx} = e_{yy} = q_{13}(P^{\mathrm{s}})^2$ and $e_{zz} = q_{33}(P^{\mathrm{s}})^2$ as well as $e_\theta = (q_{33} - q_{13})(P^{\mathrm{s}})^2$ and $e_\varepsilon = 0$. The resulting splitting of the Jahn–Teller states is given by

$$\tfrac{3}{2} V_{\mathrm{S}} e_\theta = \tfrac{3}{2} V_{\mathrm{S}} (q_{33} - q_{13})(P^{\mathrm{s}})^2 \tag{13}$$

and gives rise to the intensity ratio of the tetragonal and orthorhombic spectra:

$$\ln\left(\frac{I_{\mathrm{t}}}{I_{\mathrm{o}}}\right) = \frac{3 V_{\mathrm{S}} (q_{33} - q_{13})(P^{\mathrm{s}})^2}{2kT}. \tag{14}$$

From the experimental powder pattern, in which the orthorhombic spectrum turns up with double intensity, the intensity ratio $\frac{I_t}{I_o} \approx 2$ was roughly estimated at $T = 50$ K. Using the values $V_s \simeq 1 \times 10^4$ cm^{-1} [12, 30, 34] and $P^s = 0.75\frac{As}{m^2}$ [1], we obtain $(q_{33} - q_{13}) \approx 2.7 \times 10^{-3}\frac{m^4}{(As)^2}$.

The shifts of the oxygen ions in the $Cr^{5+}O_6^{12-}$ complex by the JT effect have only a marginal influence on the positions of the Pb neighbours. One expects that the nearest lead nuclei of the Cr^{5+} ion are magnetically equivalent in the paraelectric phase, because the paramagnetic centre is located at the centre of the Pb cube. As a consequence of structural changes in the unit cell caused by the phase transition, the Cr^{5+} ion is shifted along the direction of the electrical polarization. By its off-centre movement the magnetic equivalence of the eight Pb nuclei is lifted.

The temperature dependence of the spectra is explained by the transition of the static to dynamic Jahn–Teller effect. If the frequencies of the reorientational motions of the centres are higher than $\frac{(g_3-g_1)\beta B}{h}$, where B is the field in the centre of the spectrum and g_3 and g_1 are the principal values of the full g tensor (table 2), a nearly isotropic seven-line spectrum with an averaged g value, $g_{av} = \frac{g_1+g_2+g_3}{3}$, is observed. The widths of SHFS lines broaden with increasing temperature until they vanish at 380 K.

An alternative to the $T_2 \otimes e$ JTE-caused tetragonal distortion of the Cr^{5+} surrounding oxygen octahedron is its deformation by a negatively charged Ti vacancy in a neighbouring elementary cell, which compensates the positively charged Cr_{Ti}^{5+}. But also an off-centred position of the Cr^{5+} ion induced by a displacement along a pseudocubic axis could be the reason for a tetragonal distortion. In both cases, the local symmetry group of the Cr^{5+} defect is C_{4v} and a linear field effect is expected. Due to the lack of the inversion centre, the electrical polarizations $\vec{P}^s$ and $-\vec{P}^s$ would induce different distortions in the defect complex and two types of spectra with different principal g values should be detected in the spectra. This conclusion is contradictory to our experiments.

6. Conclusions

Two possibilities of the incorporation of paramagnetic Cr^{5+} ions with the electron configuration $3d^1$ exist in the perovskite structure: octahedrally and quasi-tetrahedrally coordinated Cr^{5+}. In the case of the octahedrally coordinated Cr^{5+} in the ferroelectric systems $BaTiO_3$ and $PbTiO_3$ the tetragonal Jahn–Teller distortion of the $Cr^{5+}O_6^{12-}$ complex is disturbed by a quadratic field effect and the D_{4h} symmetry of the complex can be reduced, dependent on the position of the spontaneous polarization with respect to the Jahn–Teller distortion axis. In the rhombohedral phase of $BaTiO_3$, the polarization vectors are parallel to the equivalent ⟨111⟩ directions and EPR spectra with only rhombic symmetry are detected; whereas in the ferroelectric lead titanate tetragonal and rhombic Cr^{5+} spectra are simultaneously detected because the vectors of the spontaneous polarization are parallel or perpendicular to the Jahn–Teller distortion axes. Up to now the quasi-tetrahedrally coordinated Cr^{5+} could not be observed in $PbTiO_3$.

Acknowledgments

The authors thank Dr H T Langhammer (Universität Halle) for stimulating discussions and Mrs U Heinich (University of Leipzig) and C Teutloff (FU Berlin) for help by the measurements of the W-band spectra.

References

[1] Rabe K, Ahn Ch H and Triscone J M 2007 *Physics of Ferroelectrics; A Modern Perspective* (Berlin: Springer)
[2] Jaffe B, Cook W R and Jaffe H 1971 *Piezoelectric Ceramics* (London: Academic)
[3] Xu Y 1991 *Ferroelectric Materials and their Applications* (Amsterdam: Elsevier)
[4] Uchino K 2000 *Ferroelectric Devices* (New York: Dekker)
[5] Lines M E and Glass A M 2001 *Principles and Applications of Ferroelectric and Related Materials* (Oxford: Oxford University Press)
[6] Possenriede E, Schirmer O F, Albers J and Godefroy C 1990 *Ferroelectrics* **107** 313
[7] Possenriede E, Jacobs P and Schirmer O F 1992 *J. Phys.: Condens. Matter* **4** 4719
[8] Possenriede E 1992 *PhD Thesis* University of Osnabrück
[9] Böttcher R, Langhammer H T and Müller T 2009 *J. Phys.: Condens. Matter* **21** 075904
[10] Böttcher R, Langhammer H T and Müller T 2009 *J. Phys.: Condens. Matter* **21** 435901
[11] Lagendijk A, Morel R J, Glasbeek M and van Voorst J D W 1972 *Chem. Phys. Lett.* **12** 518
[12] de Jong H J and Glasbeek M 1976 *Solid State Commun.* **19** 1197
[13] de Jong H J and Glasbeek M 1978 *Solid State Commun.* **28** 683
[14] Müller K A, Blazey K W and Kool Th W 1993 *Solid State Commun.* **85** 381
[15] Kool Th W, de Jong H J and Glasbeek M 1994 *J. Phys.: Condens. Matter* **6** 1571
[16] Böttcher R, Brunner W, Milsch B, Völkel G and Windsch W 1986 *Chem. Phys. Lett.* **129** 545
[17] Bennati M and Prisner Th 2005 *Rep. Prog. Phys.* **68** 411
[18] Stoll St 2003 Spectral simulation in solid-state EPR *PhD Thesis* ETH Zürich
[19] Stoll St and Schweiger A 2005 *J. Magn. Reson.* **178** 42
[20] Stoll St and Schweiger A 2007 *Biol. Magn. Reson.* **27** 299
[21] Glazer A M and Mabud S A 1978 *Acta Crystallogr.* B **34** 1065
[22] Schönau K A, Knapp M, Ehrenberg H, Eichel R A and Fuess H 2007 hasweb.desy/science/annual-report
[23] Heidler R, Windsch W, Böttcher R and Klimm C 1990 *Chem. Phys. Lett.* **175** 55
[24] Böttcher R, Erdem E, Langhammer H T, Müller T and Abicht H-P 2005 *J. Phys.: Condens. Matter* **17** 2763
[25] Erdem E, Böttcher R, Gläsel H-J and Hartmann E 2005 *Magn. Reson. Chem.* **43** 174
Erdem E, Matthes A, Böttcher R, Gläsel H-J and Hartmann E 2008 *J. Nanosci. Nanotechnol.* **8** 702
[26] Schläfer H L and Gliemann G 1969 *Basic Principles of Ligand Field Theory* (New York: Interscience)
[27] Laguta V V, Antimirova T V, Glinchuk M D, Bykov I P, Rosa J, Zaritskii M and Jastrabik L 1997 *J. Phys.: Condens. Matter* **9** 10041
[28] Abragam A and Bleaney B 1970 *Electron Paramagnetic Resonance of Transition Metal Ions* (Oxford: Clarendon)
[29] Kool Th W and Glasbeek M 1979 *Solid State Commun.* **32** 1099
[30] Kool Th W and Glasbeek M 1991 *J. Phys.: Condens. Matter* **3** 9747
[31] Faughnan B W 1972 *Phys. Rev.* B **5** 4925

[32] Scharfschwerdt R, Mazur A, Schirmer O F, Hesse H and Mendricks S 1996 *Phys. Rev.* B **54** 15284
[33] Schirmer O F, Kool Th W, Lenjer S and Maiwald M 2005 *Phys. Status Solidi* c **2** 124
[34] Lenjer S 1999 *PhD Thesis* University of Osnabrück
Lenjer S, Schirmer O F, Hesse H and Kool Th W 2002 *Phys. Rev.* B **66** 165106
[35] Schwartz R W, Wechsler A B and West L 1995 *Appl. Phys. Lett.* **67** 1352
[36] Ham F S 1972 *Electron Paramagnetic Resonance* ed S Geschwind (New York: Plenum)
[37] Strukov B A and Levanyuk A P 1998 *Ferroelectric Phenomena in Crystals: Physical Foundations* (Berlin: Springer)
[38] Pake G E and Estle T E 1973 *The Physical Principles of Electron Paramagnetic Resonance* (Cambridge, MA: Benjamin)
[39] Haussühl S 2007 *Physical Properties of Crystals: An Introduction* (Weinheim: Wiley–VCH)